Received: 28 April 2017 | Revised: 18 June 2017 | Accepted: 18 June 2017

DOI: 10.1002/er.3811

RESEARCH ARTICLE

WILEY INTERNATIONAL JOURNAL OF ENERGY RESEARCH

Modeling and performance analysis of duck-shaped triboelectric and electromagnetic generators for water wave energy harvesting

Zia Saadatnia[1] | Ehsan Asadi[2] | Hassan Askari[2] | Jean Zu[1] | Ebrahim Esmailzadeh[3]

[1] Department of Mechanical and Industrial Engineering, University of Toronto, 5 King's College Road, Toronto, ON M5S 3G8, Canada

[2] Department of Mechanical and Mechatronics Engineering, University of Waterloo, 200 University Ave West, Waterloo, ON N2L 3G1, Canada

[3] Faculty of Engineering and Applied Science, University of Ontario Institute of Technology, 2000 Simcoe St. N. Oshawa, Oshawa, ON L1H 7K4, Canada

Correspondence
Zia Saadatnia, Department of Mechanical and Industrial Engineering, University of Toronto, 5 King's College Road, Toronto, ON M5S 3G8, Canada.
Email: zsaadat@mie.utoronto.ca

Summary

Triboelectric nanogenerator (TENG) is a newly proposed technology for effectively converting mechanical energy into electricity. Triboelectric nanogenerator has shown a great potential for harvesting the clean and abundant energy of ocean waves. Recently, a duck-shaped TENG device has been proposed as a lightweight, cost-effective, highly stable, and efficient system for scavenging the existing energy in water waves. In this paper, a detailed investigation on the performance of the duck-shaped TENG is presented. Then, a comparative analysis between the TENG device and an equivalent electromagnetic generator (EMG) for wave energy harvesting is performed. The electric output characteristics of both techniques under various mechanical and electrical conditions are obtained. The analysis demonstrates that at a low operating frequency of 2.5 Hz, the TENG and EMG achieve the peak power density of 213.1 and 144.4 W/m^3, respectively. The present paper provides guidance for design and optimization of hybrid TENG and EMG technology toward scavenging the blue energy.

KEYWORDS

electromagnetic, nanogenerator, triboelectric, wave energy

1 | INTRODUCTION

With the limited resources of existing fossil fuels and related environmental effects, the demands for alternative energy sources have been increased in the past decades. Therefore, there has been a great interest toward the development of the novel energy harvesting technologies for extracting the energy of clean and renewable resources such as wind,[1] solar,[2] ocean,[3] and geothermal.[4] Among them, existing energy in the motion of water waves is a highly clean and widely distributed source around the globe.[5] Wave energy is conventionally converted to electricity by means of piezoelectric and electromagnetic generators (EMGs).[3] However, such clean energy has not been exploited properly due to various issues associated with EGM such as low frequency nature of waves, costly and bulky EMG systems, difficult portability and deployment of converters, and environmental impacts.[6] Triboelectric nanogenerators (TENGs) have been recently introduced as efficient devices for converting the mechanical energy of water waves into electricity.[7] Triboelectric nanogenerator is based on the concept of the contact electrification in conjunction with electrostatic induction to effectively scavenge the mechanical energy of low-frequency excitations.[8-10] Triboelectric nanogenerator is fundamentally made of thin film polymeric materials proposing a very lightweight, environmentally friendly, low cost, and reliable device for energy generation.[11-14] Due to such attractive attributes, TENG has been applied in numerous applications such as human body motion,[15-17] wind power,[18-22] water motion,[23,24] mechanical impact, and vibration.[25-29]

Various TENG devices for harvesting water wave energy have been introduced in the literature.[30] Such devices use different configurations such as wavy-shaped structures,[31] rolling cylinders and spheres,[32,33] direct

 Copyright © 2017 John Wiley & Sons, Ltd.

liquid-solid contact models,[34] and hybrid TENG and EMG mechanisms.[35-39] There exist significant challenges in the design of TENG wave energy harvesters including quick charge dissipation by present water in the direct water-solid contact devices, ineffective device agitation owing to intermediate parts, frequency mismatch with low-frequency waves, and device instability under harsh environment.[33] Table 1 shows a brief summary of the conventional and recent technologies based on piezoelectric, electromagnetic, and triboelectric mechanisms for water wave energy harvesting.[3,48]

To address the aforementioned challenges, we recently presented a novel and efficient TENG design for the purpose of wave energy harvesting that functions based on the oscillating Salter's duck.[23] Due to the unique structure, the duck was able to extract nearly 80% of the mechanical energy in water waves. By performing experimental analysis, we obtained the open-circuit voltage (*Voc*) of 325 V, short-circuit current (*Isc*) of 65 μA, and maximum output power of 0.455 W/m^2 for the duck-shaped TENG.[23] Although the device has shown a promising potential for wave energy harvesting, the power generation process and the device performance under different physical and geometrical conditions are yet unclear. Detailed understanding of the device working mechanism will significantly assist us for predicting the electrical output, enhancing the design, and optimizing the TENG device toward practical applications in wave energy harvesting. In addition, the EMG technique can be used for an equivalent duck-shaped configuration. A quantitative analysis between the TENG and EMG methods is not available for water wave energy harvesting. Therefore, providing a comparative analysis between the performances of the 2 methods and conjunction operation of them is essential for future blue energy applications.

TABLE 1 Review of piezoelectric, electromagnetic generator, and triboelectric nanogenerator water wave energy harvesting mechanisms

Technology	Mechanism	
Electromagnetic generator	Linear generator[40]	
	Rotary generator	Hydraulic[41]
		Wells turbine[5]
		Mechanical[3]
Piezoelectric harvester	Flow-induced vibration by wave current[42]	
	Water wave motion	Flexible membrane[43]
		Cantilevers excited by heave/pitch[44]
		Fixed device at ocean bottom[45]
	Water impact and sloshing[46]	
Triboelectric nanogenerator	Direct water-solid contact mechanism[34]	
	Fully enclosed devices	Rolling spherical/cylindrical[32,33]
		Ball collision mechanism[31]
		Other designs[47]
	Hybridized triboelectric-electromagnetic system[30]	

The present work firstly provides a comparative study on the performance of TENG and EMG based on the oscillating Salter's duck for harvesting water wave energy.[49] We propose systematic theoretical models for both types of energy harvesters to obtain corresponding electrical outputs under different dynamics. With considering set parameters, we conduct and compare the output characteristics of the 2 energy harvesters such as *Voc*, *Isc*, voltage/current responses to external loads, and output powers. Based on the obtained results, we propose conjunction operation of the TENG and EMG generators for effectively converting the kinetic energy of water waves into electricity. The novel findings of this study can be summarized in the following points:

- Electrical output characteristics of the TENG and EMG harvesting units under various dynamical and electrical conditions.
- Frequency response analysis of the 2 harvesters and optimum frequency ranges for better performances.
- Optimum resistances for obtaining maximum output powers and effect of optimum resistances on the output currents and voltages.
- A demonstration for the performance enhancement of the hybridized energy harvester compared to the single TENG or EMG harvester.

Therefore, the utilization of the 2 energy harvesters in conjunction with the mechanism of the duck exhibits a great potential for powering various systems from small scales such as wireless sensors and aquatic environment monitoring devices toward larger scales like household consumptions.

2 | MODELING

Figure 1A represents the schematic configuration of the oscillating Salter's duck under an incident wave.[50] The duck is an efficient offshore energy convertor and known as a terminator-type harvester where the device is perpendicular to beam waves.[3] The unique duck-shaped structure shows a highly efficient dynamic behavior for scavenging the wave energy so it was selected for the proposed energy harvester. When a wave moves toward the structure and passes, the rear section of the duck does not transmit the incident wave downstream and the front section encountering the wave reflects only a little portion of the wave energy.[51] In addition, the structure will fall into the original position as the wave passes due to the location of gravity center. Using fluid-solid interaction analysis, a comprehensive study on the duck-shaped dynamic behavior under different traveling wave parameters was conducted in the previous study.[23]

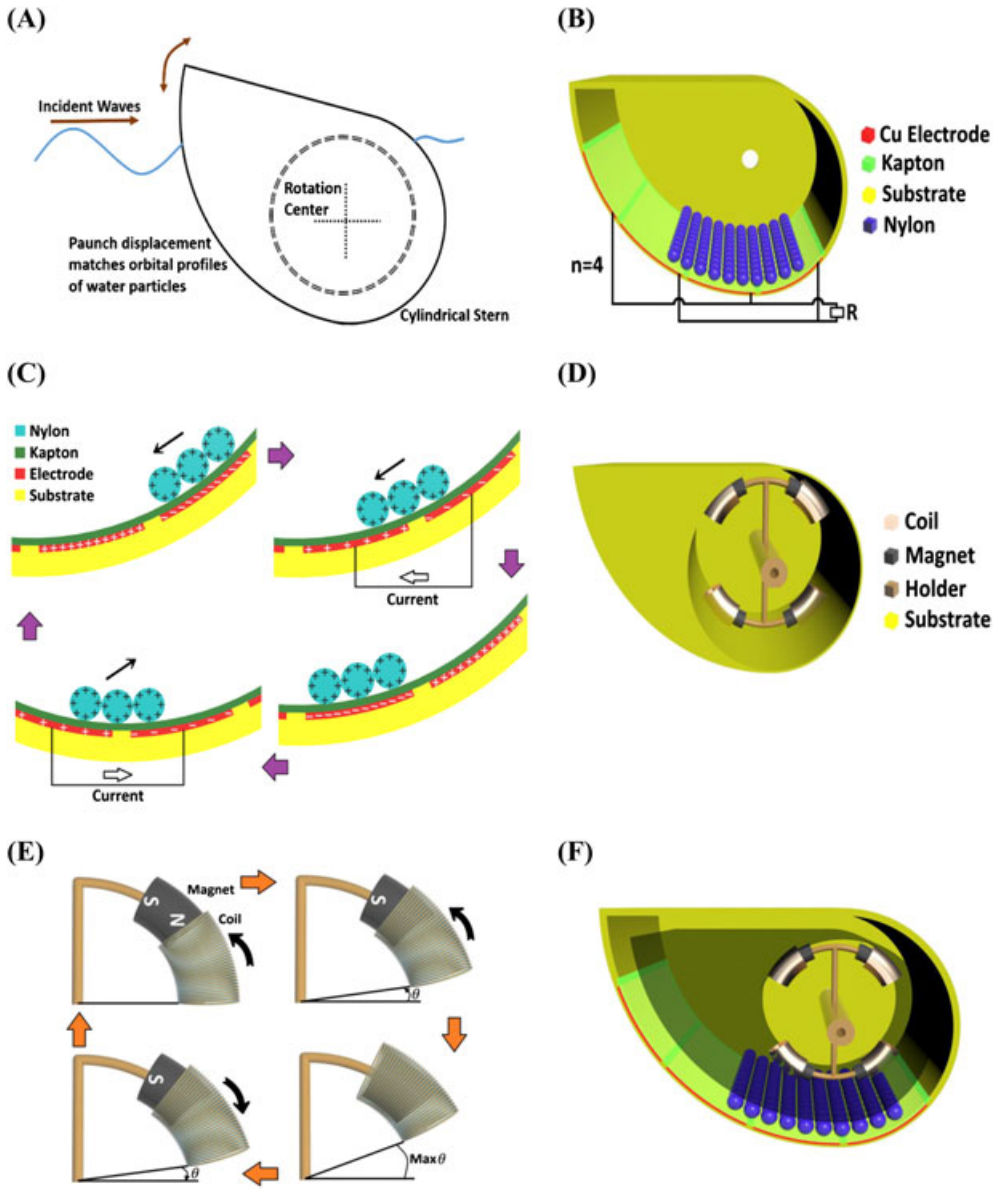

FIGURE 1 A, Schematics of Salter's duck energy harvester. B, Duck-shaped rolling freestanding triboelectric nanogenerator (TENG) model for n = 4. C, Working principle of the TENG model. D, Duck-shaped electromagnetic generator (EMG) model. E, Working principle of the EMG model. F, Coupled duck-shaped TENG-EMG energy harvester [Colour figure can be viewed at wileyonlinelibrary.com]

According to the obtained results, the duck undergoes an oscillatory pitch motion when facing normal waves. The structure ideally oscillates around an axis parallel to the incident waves where the frequency and amplitude of the oscillation is dependent to the wave dynamic characteristics. Indeed, the structure will fall into a regular harmonic motion after a few seconds, as seen in the past work.[14] Therefore, we consider this type of motion as the operating condition for the proposed energy harvester to analyze the power generations and extract the output characteristics of the system. It should be noted that the most effective parameter on the energy harvester behavior is the frequency of oscillation, which is taken as the major control parameter in the presented analysis.

2.1 | TENG model

Figure 1B depicts the design of the duck-shaped wave energy harvester based on rolling freestanding TENG mechanism.[52] The device contains rolling nylon balls, which freely slide over the Kapton layer under the oscillation of the duck and the Kapton layer covers pairs of copper electrodes, which are connected in parallel. Figure 2C shows the working mechanism of the device when the balls move over the top layer. The detailed information related to the working principle, materials selection, balls filling ratio, layers dimensions, fabrication device, and test are available in the literature.[23]

We conduct a theoretical study using FEM in COMSOL Multiphysics software package to investigate the electrical

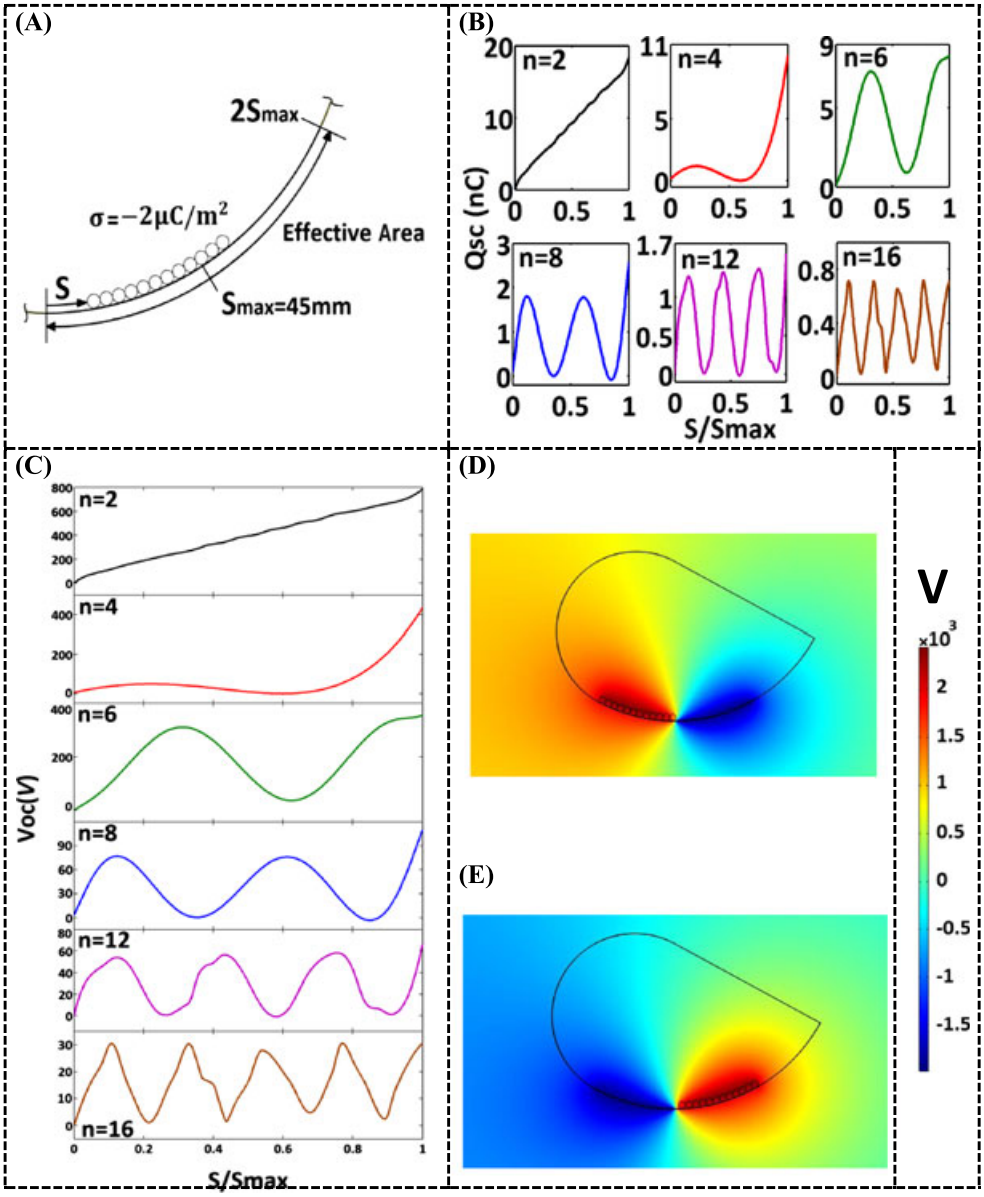

FIGURE 2 A, FEM model of the duck-shaped rolling freestanding triboelectric nanogenerator. Effect of the electrode numbers (n) on calculated B, transferred charge *Qsc* and C, open-circuit voltage *Voc*. D and E, Electric potential distribution for various balls displacement when $n = 2$ [Colour figure can be viewed at wileyonlinelibrary.com]

generation process and the output characteristics of the duck-shaped TENG. Figure 2A shows the FEM model of the device when the balls move over the effective layer, which includes the electrodes and Kapton inside the duck.

The Kapton layer covers 2 groups of interdigitated electrodes, which are placed with a similar periodicity. In each group, the electrodes are connected to each other and then connected to an external load to create a parallel connection. The total number of electrodes should be an even number so that equal numbers of electrodes are placed in the 2 electrode groups. To study the effect of electrode size on the device performance, the total effective length of electrodes was kept constant and the number of electrodes were changed from $n = 2$ to $n = 16$. Figure 1B shows a typical case when $n = 4$. For the theoretical study and based on the fabricated device, we considered a duck with 95-mm diameter of its rear section and 4-mm-diameter rolling balls. Accordingly and to perform a standard analysis, we fixed the total effective length of the electrodes at 90 mm while we changed the number of electrodes from $n = 2$ to $n = 16$, as stated. It should be noted that in all cases, the gap between 2 consecutive electrodes was taken as 1 mm. We calculated the electrical characteristics of the device such as the potential charge distribution, open-circuit voltage *Voc*, and transferred charge in short circuit condition *Qsc*, when the balls roll from the left end to the right end of the effective layer. We assigned the total surface charge density at each electrode equal to zero to maintain the open-circuit boundary condition. Also, we applied similar

electric potential on the electrodes to create short circuit boundary condition. In addition, we considered a 2D simulation due to the large depth dimension of the layer in comparison with the layer's thickness (ie, ≤200 μm). Based on the triboelectricity of nylon and Kapton, we assumed a uniform triboelectric charge density of −2 μC/m^2 on the Kapton while we selected the charge density of nylon balls so that the charge conservation was maintained. Similar to the literature, we selected the magnitude of charge density as the only assumption in the simulation.[53]

Figure 2B shows the variation of transferred *Qsc* when the position of rolling balls *S* changes from zero to the maximum value *Smax*. *S* indicates the relative displacement of rolling balls with respect to the effective layer of the duck. The effect of electrode numbers on *Qsc* is also depicted in the figure. The maximum transferred charge occurs when $n=2$ as the magnitude of transferred charge increases with respect to the displacement. Figure 2C illustrates the calculated open-circuit voltage versus the balls displacement for various electrode numbers. The value of *Voc* shows more oscillating trend as the number of electrode increases while the peak value of *Voc* decreases with the number of electrodes. This behavior can be attributed to the number of interdigitative electrode units. The maximum magnitude of *Voc* is 0.8 kV when the number of electrodes *n* is equal to 2. As a result, we observed the best performance for $n=2$ and, consequently, we use this case as the ideal configuration for further analysis of the duck-shaped TENG. Figure 2D,E shows the open-circuit electric potential distribution when $n=2$ for different rolling displacement *S*. When $S=0$, the balls are fully in contact with the left electrode. It is clear that the electric potential increases as the balls roll toward the right electrode and the maximum values are reached when the balls are in full contact with right electrode, ie, $S=Smax$. To analyze the electrostatic and load circuit response of the duck-shaped TENG device, we used the lumped parameter equivalent circuit model for $V-Q-S$ relationship of the TENG system.[54] Figure 3A shows the equivalent circuit containing the TENG electrical generation unit as well as the external load section.[54] The parameter *C* indicates the inherent capacitance of the duck-shaped TENG and can be calculated using the following relationship:

$$C(S) = \frac{Q_{SC}(S)}{V_{OC}(S)} \tag{1}$$

According to the results of FEM simulation, we obtained the variations of *Voc* and *Qsc* with respect to the relative displacement *S*. Afterward, we implemented continuous fraction interpolation to create the relationships of *Voc*(*S*) and *Qsc*(*S*) in the entire region of *S*.[53] Then, we obtained the governing equation of the inherent capacitance with respect to *S* based on Equation 1. Since we already calculated the governing equations of *Voc*(*S*) and *C*(*S*), we were able to analyze the output characteristics of the duck-shaped TENG by means of a load circuit model. Considering the case where a resistance is taken as the external load. Using Kirchhoff's law, the electrical governing differential equation ($V-Q-S$) of the system is constructed as

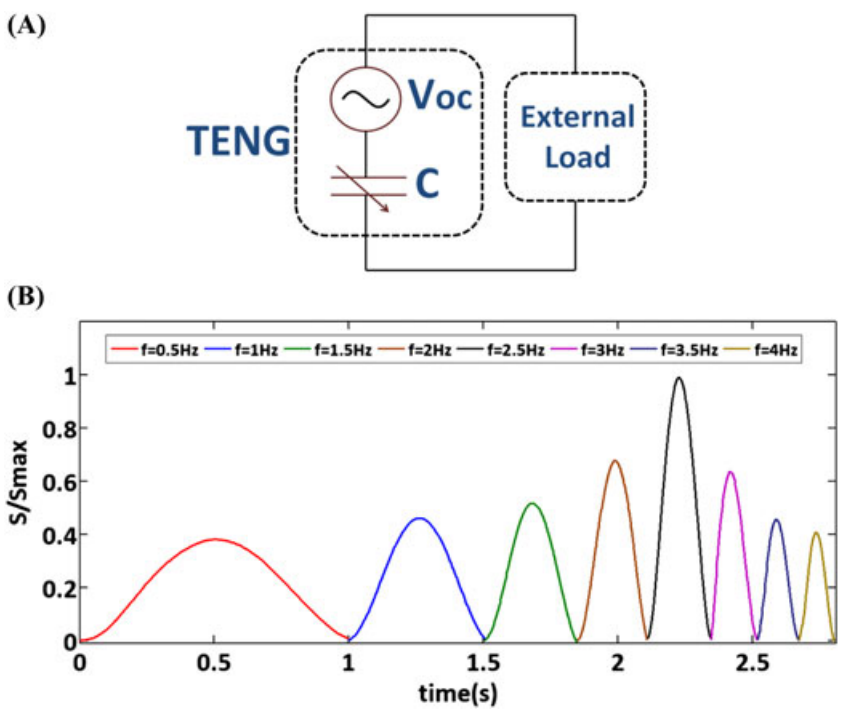

FIGURE 3 A, First-order lumped parameter equivalent circuit model of a triboelectric nanogenerator device. B, Average relative displacement curves for different oscillation frequencies [Colour figure can be viewed at wileyonlinelibrary.com]

$$R\frac{dQ}{dt} = V = -\frac{1}{C(S)} \times Q + V_{OC}(S) \tag{2}$$

Equation 2 shows a first-order differential equation, which should be solved for calculating the equations of $Q(t)$, $V(t)$, and $I(t)$ as the outputs of the duck-shaped TENG. Solving above first-order differential equation, the solution of output charge is

$$Q(t) = \frac{1}{R}\exp\left(-\int_0^t \frac{dt}{RC(S(t))}\right)\left\{\int_0^t V_{OC}(S(t))\exp \times \left(\int_0^t \frac{dy}{RC(S(y))}\right)dt\right\} + C_0\exp\left(-\int_0^t \frac{dt}{RC(S(t))}\right), \tag{3}$$

where C_0 is the integral constant. Applying the periodic boundary condition by setting $Q(t=0)=Q(t=T)$, C_0 can be obtained and therefore the solution is fully found. Also, $V(t)$ is simply found using the relationship presented in Equation 2 as

$$V(t) = -\frac{1}{C}Q(t) + V_{OC}, \tag{4}$$

and the corresponding current is

$$I(t) = \frac{V(t)}{R}. \tag{5}$$

Therefore, we could theoretically obtain the electrical output characteristics of the duck-shaped TENG. The only important parameter, which should be calculated, is the relative displacement of balls with respect to the effective layer inside the duck, ie, $S(t)$. The variation of S with respect to time is highly related to the dynamic behavior of the duck. To calculate $S(t)$ and due to the multiple units of moving elements, we needed to perform a comprehensive multibody dynamics analysis. Owing to the use of multiple balls inside the duck, understanding the dynamical behavior of the rolling balls under the duck pitch motion is complicated. For this purpose, we modeled the system dynamics using MSC ADAMS software and we performed the multibody dynamic analysis under various motion conditions. According to this model, we restricted the rotation center of the duck to only one degree of rotation, ie, the pitch motion. The balls located inside the duck can roll along the duck inner layer considering frictions between the balls and duck inner layer as well as balls interactions. Note that the friction parameters are different between the contacts of balls and the inner layer and the balls interactions. Subsequently, we applied harmonic rotations around the rotation center of the duck for various operating frequencies. Using MSC ADAMS software, we extracted the average relative displacement of the balls versus the effective duck layer for different motion conditions. To simulate the pitch motion of the duck when facing water waves, we applied various oscillations based on the frequencies and amplitudes used in the literature.[23] Then, we evaluated the relative displacements of balls and calculate the average displacement to obtain $S(t)$. Figure 3B shows the ratio of average S to the maximum effective S ($S/Smax$) for different oscillation frequencies in a full cycle. It is clear that the peak relative displacement is small for lower frequencies and then rises by increasing the frequency. The maximum peak value of S is at the frequency of 2.5 Hz and then the peak value decreases by enhancing the oscillation frequency. This might be attributed to the balls' motion resonance with the duck oscillation at this frequency. By further observation of the average relative displacement curves, we could reasonably estimate the function of $S(t)$ as

$$S(t) = \frac{S_{peak}}{2}(1-\cos(\omega t)), \tag{6}$$

where S_{peak} and ω denote the peak displacement and frequency of the cycle, respectively. Therefore, we determined all required parameters for investigating the power generation process and output characteristic of the duck-shaped TENG.

2.2 | EMG model

The EMG component of the duck-shaped system operates based on the Lenz-Faraday's law of induction.[55] As stated by this law, a change in the magnetic flux in a closed circuit produces an electromotive force (V_{EMG}) in the circuit. The produced voltage is proportionally related to the rate of the magnetic flux change and further its direction is opposing the changes. For an electromagnetic coil with N turns, V_{EMG} is calculated by

$$V_{EMG} = -\sum_{i=1}^{N}\frac{d\varphi_i}{dt}, \tag{7}$$

where φ_i is the magnetic flux in the ith turn of the coil. The structure of the EMG component is presented in Figure 1D. The EMG component includes 4 units of stationary magnets and 4 units of moving electromagnetic coils. The magnets and coils are an arc of solid and thin-walled toroidal shapes, respectively. Neodymium N42 magnet series were selected here, which are one of the highest grades of magnets and also are available in the market. The Neodymium N42 magnet is able to generate a maximum magnetic field of 0.18791 T in the coil wires.[55] The relative motion of magnets and coils is illustrated in Figure 1E. The magnets are secured to a stationary frame while the coils are mounted on the lateral surface of the salt duck, and thus moving radially as the salt duck rotates. This relative motion changes the location of the magnets inside the coils and thus changes the magnetic flux of the coils, producing V_{EMG}. Based on Faraday's law, the time

derivative of magnetic flux in the ith turn of wire (φ_i) is equal to $B_n VL$, where B_n, V, and L are the component of the magnetic flux density that is normal to the wire turn plane, relative velocity of magnet and coil wire turn, and length of the wire turn, respectively. By obtaining the values of B_n, and L from COMSOL FEM and geometry, respectively, one can calculate the electromotive force for each wire turn (V_{EMG_i}) and thus calculate the total electromotive force (V_{EMG}) using Equation 7. In summary, the rate of the magnetic flux change is proportional to the velocity of the rotation. Therefore, the formula for calculating V_{EMG} becomes

$$V_{EMG} = -k_v \frac{dS(t)}{dt}, \tag{8}$$

where $S(t)$ is the displacement, and k_v is called the machine (or voltage) coefficient of EMG component, and its magnitude depends on the geometrical dimensions as well as the magnets strength. It should be noted that the value of k_v does not remain constant for all the coil sections and, in fact, it changes for different wire turns. Here, for simplicity, a single k_v is used in the equations; however, in the calculations performed to obtain V_{EMG}, different k_v are used for different coil wire turns that are obtained from COMSOL FEM.

The induced current (i) inside each coil then can be evaluated using the following equation:

$$L_{coil}\frac{di}{dt} + (R_{coil} + R_{load})i = V_{EMG} = -k_v \frac{dS(t)}{dt}, \tag{9}$$

where L_{coil} and R_{coil} are inductance and resistance of the coils, respectively, and R_{load} is the resistance of the load connected to the coils. Accordingly, the EMG regenerated power (P_{EMG}) is found as

$$P_{EMG} = R_{load} i^2. \tag{10}$$

To find the output of the coils and the regenerated power, the EMG component is modeled using FEM. Figure 4 shows a cross section (and magnified view) of the FEM model, provided by COMSOL software. As can be seen by Figure 4, the magnitude and direction of the magnetic flux density in each section of the coil depends on the relative position of magnet and the coil.

2.3 | Output characteristics

We evaluated the output performance of the TENG and EMG wave energy harvesters for different mechanical and electrical working conditions. Figure 5A,B depicts the time response of *Voc* for different operation frequencies for the TENG and EMG, respectively. For the TENG, the maximum *Voc* is obtained nearly 390 V at 2.5 Hz as the optimum frequency. This is attributed to the maximum relative displacement of

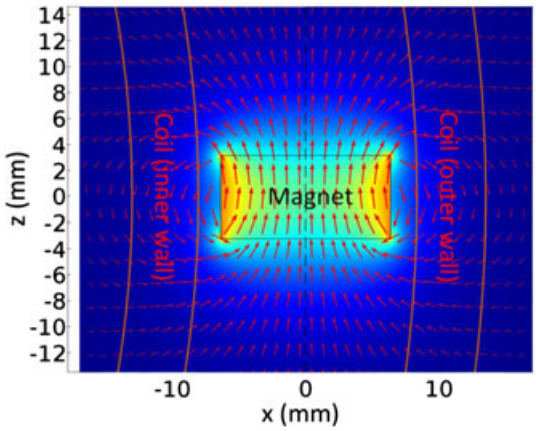

FIGURE 4 A cross section of the FEM model obtained for the electromagnetic generator. The colors represent the magnetic flux densities and the arrows show the direction of magnetic flux density at each location. The magnet and coil boundaries are shown using black and red solid lines, and the symmetry line of the magnet is shown by black dashed line [Colour figure can be viewed at wileyonlinelibrary.com]

rolling balls on the effective area of the TENG and resonance of the balls inside the device. For the EMG, *Voc* is proportional to the frequency and clearly shows an increasing trend with the operation frequency.

Figure 5C,D shows the effective values of output voltage and current for the 2 generators with the variation of external resistance at 2.5 Hz operation frequency. It is clear that the output voltage increases by the external load until it saturates in a specific value at very large resistances. Such large resistances can be considered as the open-circuit condition where the TENG and EMG obtain nearly 390 V and 180 mV, respectively. The output current decreases by increasing the resistance due to the ohmic loss. The maximum current is obtained when the external resistance is very small referring to the short circuit condition where the TENG and EMG achieve nearly 7.2 μA and 0.12 A, respectively. Figure 5E represents the output power density of the 2 generators for different resistive loads at 2.5 Hz oscillation. The optimum external resistance of TENG is $R_{opt-TENG} = 280$ MΩ where gives the power density of 213 W/m^3 at the frequency of 2.5 Hz. The optimum resistance of EMG is $R_{opt-EMG} = 1.5$ Ω in which the power density of 144 W/m^3 is obtained at the same operating frequency. Figure 5F shows a very important result, ie, the effect of oscillation frequency on the output power density of the 2 devices. It is clear that for very small frequencies, EMG shows a better behavior owing to the small motion of rolling balls inside the TENG device. However, the TENG shows a superior behavior in a specific frequency domain, which is close to the wave motion frequencies. This domain should be considered for the design of wave energy harvesting devices using the TENG mechanism. Therefore, as the frequency range of water waves is around 2 Hz,[56] the

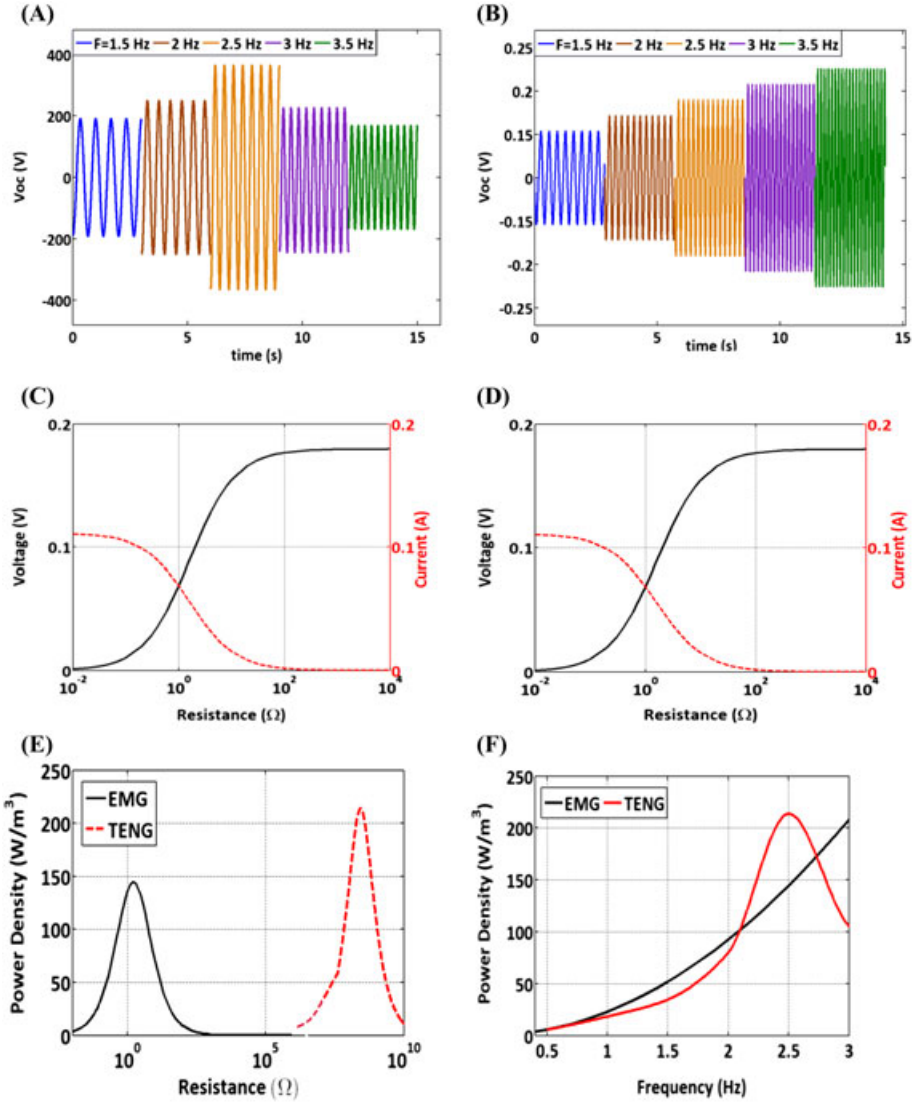

FIGURE 5 *Voc* response for different oscillation frequencies: A, TENG and B, EMG. The dependence of output voltage and current on the external loads: C, TENG and D, EMG. E, The relationship between the output power and the resistance of the external load in both methods. F, Output performance comparison between the EMG and TENG wave energy harvester at low frequency of excitations. EMG, electromagnetic generator; TENG, triboelectric nanogenerator [Colour figure can be viewed at wileyonlinelibrary.com]

use of proposed TENG harvester in conjunction with the EMG device is remarkably suitable for energy harvesting applications. For larger frequencies, the performance of the EMG is enhanced unlike the TENG device.

For further practical investigation of the 2 generators, we also studied the output characteristics of the TENG and EMG devices considering the effect of the optimum external resistance R_{opt}. Here, we defined a relative resistance $Rt = R/R_{opt}$ indicating the ratio of arbitrary external resistance to the optimum resistance for each generator. Figure 6A,B shows the time domain output voltages of the 2 generators for various frequency ratios. Figure 6C,D also depicts the time domain output currents of the 2 generators for various Rt. We observed that for both generators, the output voltage relatively enhances with the value of Rt while the output current is inversely proportional with Rt. We also studied the effect of the operation frequency on the output voltage and current of the TENG and EMG wave energy harvesters when the external resistances are equal to the corresponding R_{opt} of the 2 generators. Figure 6E illustrates the variation of both voltage and current with respect to the frequency for the TENG when $R = R_{opt-TENG}$. At the optimum frequency of 2.5 Hz, the peak values of voltage and current are obtained as 263.5 V and 4.71 μA, respectively. For the EMG energy harvester, the output voltage and current relatively increased by the frequency for the case $R = R_{opt-EMG}$, as shown in Figure 6F. As a result, the maximum voltage of 0.21 V and maximum current of 0.13 A is achieved at the operation frequency of 3.5 Hz.

To further verify the theoretical modeling and predictions, we conducted a comparison between the theoretical results of the TENG wave energy harvester with the

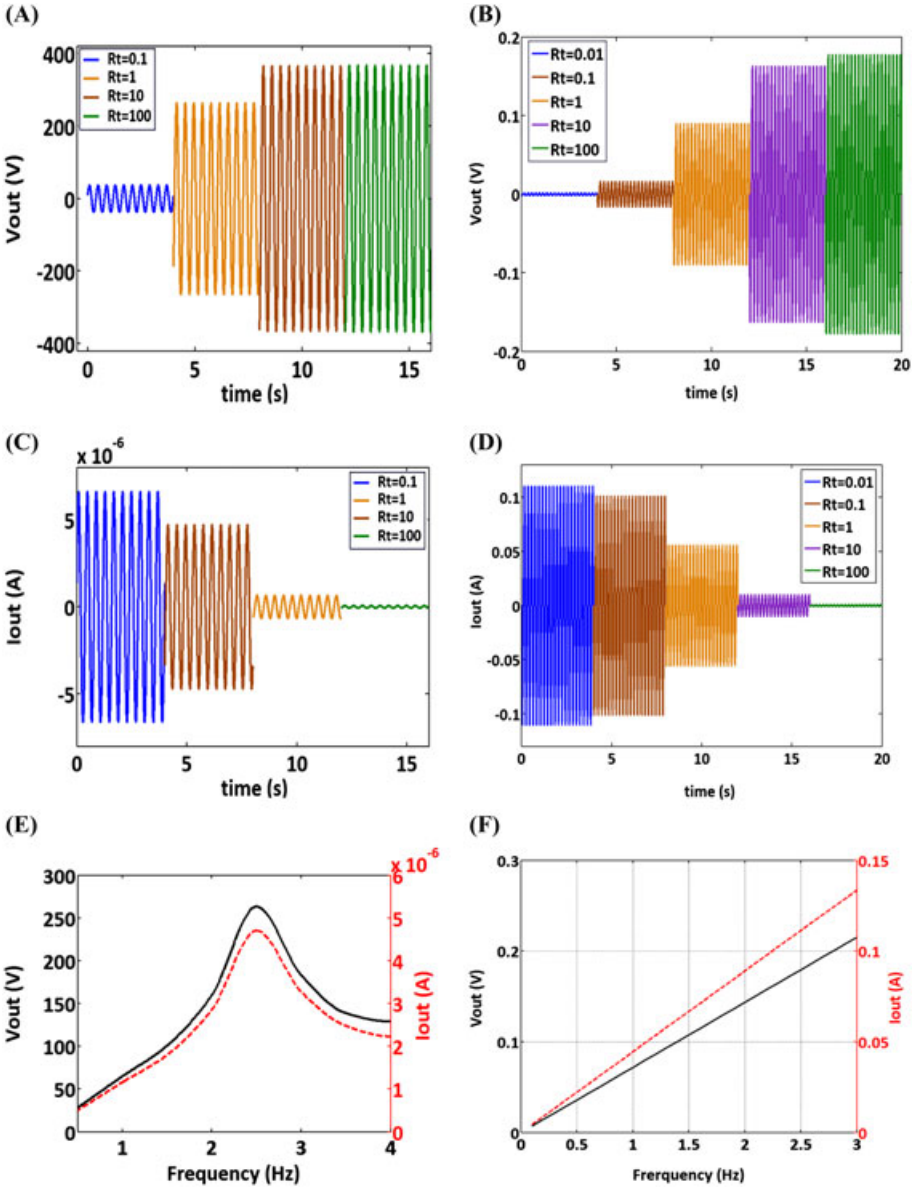

FIGURE 6 Output voltage response for different *Rt*: A, triboelectric nanogenerator (TENG) and B, electromagnetic generator (EMG). Output current response for different *Rt*: C, TENG and D, EMG. The effect of frequency on the out performance at the optimum external resistance: E, TENG and F, EMG [Colour figure can be viewed at wileyonlinelibrary.com]

corresponding experimental results obtained in the previous study.[23] For this purpose, we applied different motions to the duck TENG wave harvester similar to the experimental test conditions and calculated the output *Voc* for several periods. Figure 7A depicts the *Voc* time histories of the harvester under various frequencies of motion. Further discussions related to the device testing and measurements are presented in the reported work.[23] Accordingly, we observed that the output voltage exhibits a harmonic behavior from the minimum to the maximum magnitudes of *Voc*. For small frequencies, *Voc* is low and then increases by increasing the motion frequency. We observed a low *Voc* in small frequencies, which increases as the operating frequency increases. The maximum output *Voc* occurs at 2.5 Hz excitation, which is around 150 V. Then, *Voc* starts to decrease by increasing the excitation frequency. This behavior is attributed to the relative motions of the balls on the effective layer of the device for different frequencies and resonant behavior at a certain frequency. The results show a very reasonable correlation with the experimental results of the previous report.[23] We noticed that the magnitude and trend of *Voc* are very similar to those of the experimental observations. There exist small differences between the 2 results, which can be addressed by the following points: (1) the measured data in the experiments were obtained for a multilayered duck structure; (2) the selected boundary condition for the simulations might be different from the actual values; and (3) the frequencies of experimental tests were not exactly equal to the theoretical

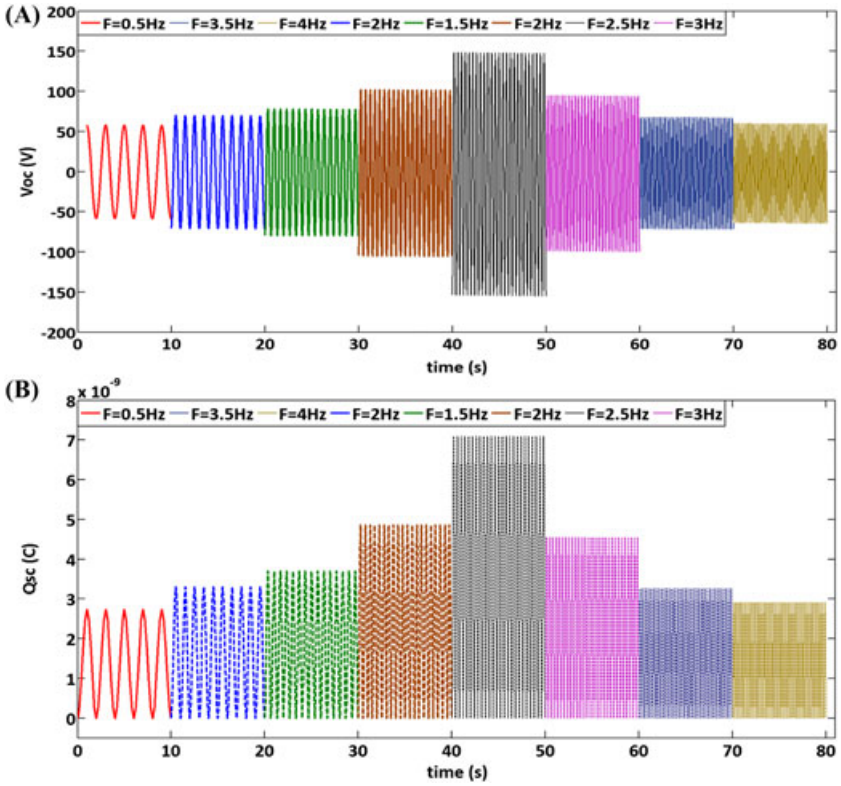

FIGURE 7 Dependence of the duck-shaped triboelectric nanogenerator outputs on different motion frequencies: A, *Voc* and B, *Qsc* [Colour figure can be viewed at wileyonlinelibrary.com]

calculation. However, the relative variation of *Voc* will not be affected by aforementioned points.

In addition, we also obtained the short circuit transferred charge (Qsc) for this case study (ie, n = 6), and we studied the effect of operating frequency on the transferred Qsc, as shown in Figure 7B. It is clear that magnitude of Qsc enhances by the frequency until reaching the resonance condition and then decreases by the frequency. Similarly, as the frequency approaches to 2.5 Hz, the rolling balls show more relative displacement and consequently further charges will be transferred in the system. The maximum amplitude of Qsc is 7.1 nC at the resonance frequency, as observed in Figure 7B.

2.4 | Conjunction operation

According to the working principles of the 2 generators, we present a coupled TENG and EMG system for effectively harvesting the wave energy. As noticed in the literature, the EMG is referred to an ideal voltage source due to a very small internal resistance and independent output voltage of the external load.[9] However, the TENG exhibits an ideal current source owing to a very large internal resistance and independent output current of the external load. We coupled the 2 generators through an electrical circuit to analyze the capability of the system for efficiently harvesting the mechanical energy of waves. Figure 8A represents a schematic view of the coupled device using rectification units, storage capacitors, and switches. We evaluated the charging process of a 40 μF capacitor by means of the single TENG, single EMG, and the coupled system for different frequencies of wave motions. Figure 8B shows the charging voltage curves of the capacitor at a typical frequency of motion, ie, 2.5 Hz. Accordingly, the single EMG charges the capacitor very quickly until it reaches a specific value and then the charging voltage will saturate at that value. The TENG charges the capacitor to a large magnitude of voltage but in a considerably long time. The system with conjunction of the 2 generators can charge the capacitor to a greater voltage value in a shorter time. This means that such system will enhance the system performance in terms of the magnitude of charging voltage as well as the charging period. We also observed a similar behavior for the performance of the hybrid TENG and EMG systems in the literature.[25,35] Figure 8C illustrates the charging curves of the capacitor for various motion frequencies using only the TENG and the EMG. Figure 8D also represents the charging curves for the coupled system at different frequencies. Both figures suggest that the electrical output performance of the system is remarkably dependent to the dynamic behavior of the device. For the EMG, the output performance is enhanced by increasing the frequency of motion. However, for the TENG and the coupled system the output performance increases by the frequency until it reaches the best performances at 2.5 Hz and then decreases by increasing the frequency. Therefore, the performance of this system is suitable for low-frequency motion of water waves in real-world applications. We should note that the output of the TENG-EMG system can be further improved using

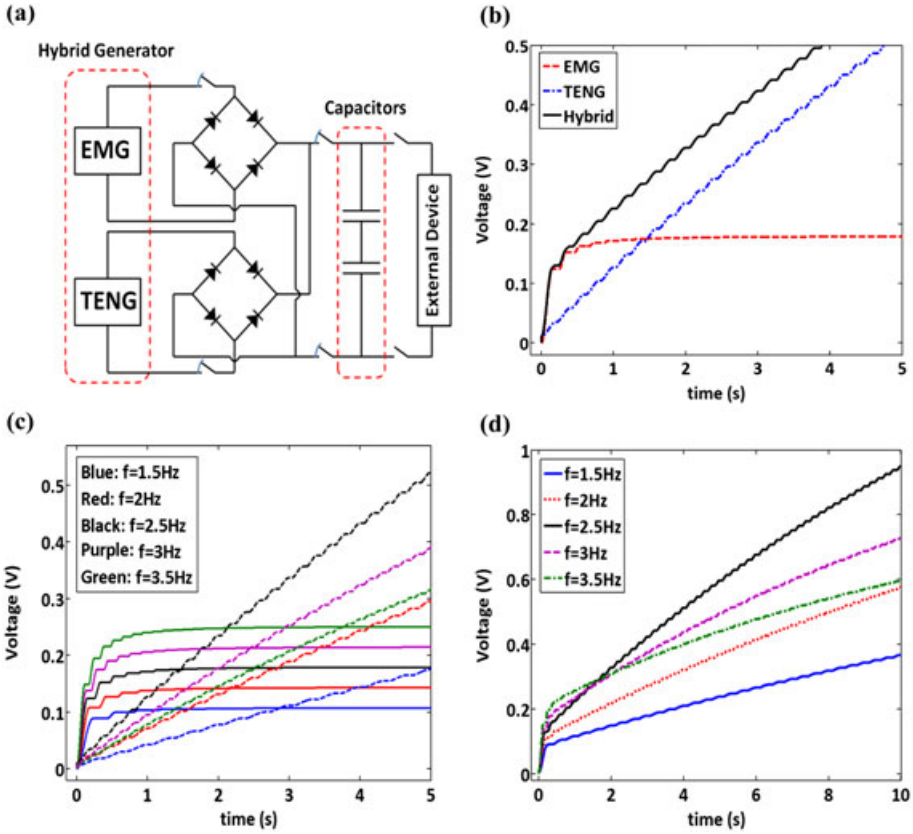

FIGURE 8 A, Schematic of the duck-shaped TENG, EMG, and coupled system for charging capacitors. B, Charging voltage curves for a 40 μF capacitor at 2.5 Hz motion with different methods. C, Effect of frequency on the charging voltage of the capacitor with the TENG (dashed lines) and EMG (solid lines). D, Effect frequency on the charging voltage of the capacitor with the coupled system. EMG, electromagnetic generator; TENG, triboelectric nanogenerator [Colour figure can be viewed at wileyonlinelibrary.com]

reported power transformed and managed systems for better matching of the TENG and EMG energy harvesters.[57,58]

We also calculated the electrical conversion efficiency of the system at 2.5 Hz motion frequency using the following relationship:

$$\eta\% = \frac{\textit{Output electrical power}}{\textit{Input mechanical power}} \times 100, \tag{11}$$

where the input mechanical power indicates the amount of power required for exerting oscillating pitch motion to the duck as

$$\text{Input mechanical power} = \textit{Applied moment} \times \text{Angular velocity}. \tag{12}$$

Using above relationships and the calculated output electrical powers, the electrical conversion efficiency of the whole device was found as $\eta \approx 58\%$. We should note that the use of conventional wave energy generators may lead to different environmental impacts owing to the leakage of hydraulic and lubricant fluids as well as structural corrosions, which are harmful for the generator surrounding area.[23] The presented device has a great potential toward clean energy harvesting from water waves. The device uses a fully insulated configuration where the triboelectric unit incorporates lightweight, environmentally friendly, and corrosion resistant polymeric materials. Also, the electromagnetic unit works based on the relative motion of magnets and coils without requiring any hydraulic fluids and heavy gear boxes. Therefore, the hybridized system can be taken as an environmental friendly energy harvester for blue energy application.

3 | CONCLUSION

We have developed theoretical models for analyzing and comparing the duck-shaped TENG and EMG devices for harvesting water wave energy. We used multibody dynamics analysis and FEM simulation to investigate the mechanical and electrical properties of the 2 generators. The electrical output characteristics of the 2 generators were evaluated for various dynamics as well as different electrical load conditions. The key findings of the papers are summarized as

- The effect of operating frequency is very critical for determining the performance of both harvesters.

- For the range of frequency from 2 to 2.75 Hz, the TENG harvester shows a superior performance over the EMG device, which is highly important for the design of the wave energy harvester.
- The role of optimum external resistance on the output characteristics of the TENG and EMG wave energy harvesters is very significant to obtain maximum output power.
- The hybridized TENG and EMG generator demonstrates a superior potential for harvesting water wave energy.

In summary, this paper proposed a comprehensive study on the performance of duck-shaped TENG and EMG wave energy convertors, which provides potential guidelines the design and improvement of blue energy harvesting systems.

REFERENCES

1. Şahin AD, Dincer I, Rosen MA. Thermodynamic analysis of wind energy. *Int J Energy Res*. 2006;30(8):553-566.
2. Ozlu S, Dincer I. Analysis and evaluation of a new solar energy-based multigeneration system. *Int J Energy Res*. 2016;40(10):1339-1354.
3. Antonio FO. Wave energy utilization: a review of the technologies. *Renew Sustain Energy Rev*. 2010;14(3):899-918.
4. Balta MT, Dincer I, Hepbasli A. Geothermal-based hydrogen production using thermochemical and hybrid cycles: a review and analysis. *Int J Energy Res*. 2010;34(9):757-775.
5. Shehata AS, Xiao Q, Saqr KM, Alexander D. Wells turbine for wave energy conversion: a review. *Int J Energy Res*. 2017;41(1):6-38.
6. Thorpe T. Harvesting the waves. Ingenia, issue13, Royal Academy of Engineering, UK. 2002.
7. Chen J, Yang J, Li Z, et al. Networks of triboelectric nanogenerators for harvesting water wave energy: a potential approach toward blue energy. *ACS Nano*. 2015;9(3):3324-3331.
8. Zi Y, Guo H, Wen Z, Yeh M-H, Hu C, Wang ZL. Harvesting low-frequency (<5 Hz) irregular mechanical energy: a possible killer application of triboelectric nanogenerator. *ACS Nano*. 2016;10(4):4797-4805.
9. Zhang C, Tang W, Han C, Fan F, Wang ZL. Theoretical comparison, equivalent transformation, and conjunction operations of electromagnetic induction generator and triboelectric nanogenerator for harvesting mechanical energy. *Adv Mater*. 2014;26(22):3580-3591.
10. Wang ZL. On Maxwell's displacement current for energy and sensors: the origin of nanogenerators. *Mater Today*. 2017; https://doi.org/10.1016/j.mattod.2016.12.001
11. Fang H, Wang X, Li Q, Peng D, Yan Q, Pan C. A stretchable nanogenerator with electric/light dual-mode energy conversion. *Adv Energy Mater*. 2016;6(18):1600829.
12. Xu W, Huang LB, Wong MC, Chen L, Bai G, Hao J. Environmentally friendly hydrogel-based triboelectric nanogenerators for versatile energy harvesting and self-powered sensors. *Adv Energy Mater*. 2016; https://doi.org/10.1002/aenm.201601529
13. Shin SY, Saravanakumar B, Ramadoss A, Kim SJ. Fabrication of PDMS-based triboelectric nanogenerator for self-sustained power source application. *Int J Energy Res*. 2016;40(3):288-297.
14. Shaislamov U, Kim Y, Kim WS, Jeong H, Lee HJ, Chun W. Hybrid operation of triboelectric nanogenerator for electricity generation by a low-temperature differential heat engine. *Int J Energy Res*. 2016; https://doi.org/10.1002/admt.2016001602016
15. Zhang K, Wang X, Yang Y, Wang ZL. Hybridized electromagnetic-triboelectric nanogenerator for scavenging biomechanical energy for sustainably powering wearable electronics. *ACS Nano*. 2015;9(4):3521-3529.
16. Yang W, Chen J, Zhu G, et al. Harvesting energy from the natural vibration of human walking. *ACS Nano*. 2013;7(12):11317-11324.
17. Jin L, Chen J, Zhang B, et al. Self-powered safety helmet based on hybridized nanogenerator for emergency. *ACS Nano*. 2016;10(8):7874-7881.
18. Chen S, Gao C, Tang W, et al. Self-powered cleaning of air pollution by wind driven triboelectric nanogenerator. *Nano Energy*. 2015;14:217-225.
19. Zhang L, Zhang B, Chen J, et al. Lawn structured triboelectric nanogenerators for scavenging sweeping wind energy on rooftops. *Adv Mater*. 2016;28(8):1650-1656.
20. Quan Z, Han CB, Jiang T, Wang ZL. Robust thin films-based triboelectric nanogenerator arrays for harvesting bidirectional wind energy. *Adv Energy Mater*. 2016;6(5):1501799.
21. Zhang B, Chen J, Jin L, et al. Rotating-disk-based hybridized electromagnetic-triboelectric nanogenerator for sustainably powering wireless traffic volume sensors. *ACS Nano*. 2016;10(6):6241-6247.
22. Zhao K, Wang X, Yang Y. Ultra-stable electret nanogenerator to scavenge high-speed rotational energy for self-powered electronics. *Adv Mater Technol*. 2016; https://doi.org/10.1002/admt.201600233
23. Ahmed A, Saadatnia Z, Hassan I, et al. Self-powered wireless sensor node enabled by a duck-shaped triboelectric nanogenerator for harvesting water wave energy. *Adv Energy Mater*. 2016; https://doi.org/10.1002/aenm.201601705
24. Ahmed A, Hassan I, Jiang T, et al. Design guidelines of triboelectric nanogenerator for water wave energy harvesters. *Nanotechnology*. 2017;28(18):185403.
25. Askari H, Asadi E, Saadatnia Z, Khajepour A, Khamesee MB, Zu J. A hybridized electromagnetic-triboelectric self-powered sensor for traffic monitoring: concept, modelling, and optimization. *Nano Energy*. 2017;32:105-116.
26. Yang J, Chen J, Yang Y, et al. Broadband vibrational energy harvesting based on a triboelectric nanogenerator. *Adv Energy Mater*. 2014;4(6):4090-4096.
27. Zhang L, Jin L, Zhang B, et al. Multifunctional triboelectric nanogenerator based on porous micro-nickel foam to harvest mechanical energy. *Nano Energy*. 2015;16:516-523.
28. Yang W, Chen J, Jing Q, et al. 3D stack integrated triboelectric nanogenerator for harvesting vibration energy. *Adv Funct Mater*. 2014;24(26):4090-4096.
29. Seol M-L, Han J-W, Park S-J, Jeon S-B, Choi Y-K. Hybrid energy harvester with simultaneous triboelectric and electromagnetic generation from an embedded floating oscillator in a single package. *Nano Energy*. 2016;23:50-59.

30. Wen Z, Guo H, Zi Y, et al. Harvesting broad frequency-band blue energy by a triboelectric-electromagnetic hybrid nanogenerator. *ACS Nano*. 2016;10:6526.

31. Yao Y, Jiang T, Zhang L, Chen X, Gao Z, Wang ZL. Charging system optimization of triboelectric nanogenerator for water wave energy harvesting and storage. *ACS Appl Mater Interfaces*. 2016;8(33):21398-21406.

32. Lin Z-H, Cheng G, Li X, Yang P-K, Wen X, Wang ZL. A multi-layered interdigitative-electrodes-based triboelectric nanogenerator for harvesting hydropower. *Nano Energy*. 2015;15:256-265.

33. Wang X, Niu S, Yin Y, Yi F, You Z, Wang ZL. Triboelectric nanogenerator based on fully enclosed rolling spherical structure for harvesting low-frequency water wave energy. *Adv Energy Mater*. 2015;5(24):1501467.

34. Zhu G, Su Y, Bai P, et al. Harvesting water wave energy by asymmetric screening of electrostatic charges on a nanostructured hydrophobic thin-film surface. *ACS Nano*. 2014;8(6):6031-6037.

35. Wang X, Wen Z, Guo H, et al. A fully packaged blue energy harvester by hybridizing a rolling triboelectric nanogenerator and an electromagnetic generator. *ACS Nano*. 2016;10(12):11369-11376.

36. Wang X, Wang ZL, Yang Y. Hybridized nanogenerator for simultaneously scavenging mechanical and thermal energies by electromagnetic-triboelectric-thermoelectric effects. *Nano Energy*. 2016;26:164-171.

37. Zhong X, Yang Y, Wang X, Wang ZL. Rotating-disk-based hybridized electromagnetic-triboelectric nanogenerator for scavenging biomechanical energy as a mobile power source. *Nano Energy*. 2015;13:771-780.

38. Guo H, Wen Z, Zi Y, et al. A water-proof triboelectric-electromagnetic hybrid generator for energy harvesting in harsh environments. *Adv Energy Mater*. 2015; https://doi.org/10.1002/aenm.201501593

39. Quan T, Wang X, Wang ZL, Yang Y. Hybridized electromagnetic-triboelectric nanogenerator for a self-powered electronic watch. *ACS Nano*. 2015;9(12):12301-12310.

40. Stelzer M, Joshi R. Evaluation of wave energy generation from buoy heave response based on linear generator concepts. *J Renewable Sustainable Energy*. 2012;4(6):063137.

41. Henderson R. Design, simulation, and testing of a novel hydraulic power take-off system for the Pelamis Wave Energy Converter. *Renew Energy*. 2006;31(2):271-283.

42. Akaydin HD, Elvin N, Andreopoulos Y. Energy harvesting from highly unsteady fluid flows using piezoelectric materials. *J Intell Mater Syst Struct*. 2010;21(13):1263-1278.

43. Mutsuda H, Watanabe R, Azuma S, Tanaka Y, Doi Y, editors. Ocean power generator using flexible piezoelectric device. ASME 2013 32nd International Conference on Ocean, Offshore and Arctic Engineering; 2013: American Society of Mechanical Engineers.

44. Viñolo C, Toma D, Mànuel A, del Rio J. An ocean kinetic energy converter for low-power applications using piezoelectric disk elements. *Eur Phys J Spec Top*. 2013;222(7):1685-1698.

45. Xie X, Wang Q, Wu N. Potential of a piezoelectric energy harvester from sea waves. *J Sound Vib*. 2014;333(5):1421-1429.

46. Athanassoulis G, Mamis K. Modeling and analysis of a cliff-mounted piezoelectric sea-wave energy absorption system. *Coupled Syst Mech*. 2013;2(1):53-83.

47. Jiang T, Yao Y, Xu L, Zhang L, Xiao T, Wang ZL. Spring-assisted triboelectric nanogenerator for efficiently harvesting water wave energy. *Nano Energy*. 2017;31:560-567.

48. Jbaily A, Yeung RW. Piezoelectric devices for ocean energy: a brief survey. *J Ocean Eng Mar Energy*. 2015;1(1):101-118.

49. Salter SH. Wave power. *Nature*. 1974;249(5459):720-724.

50. Lucas J, Salter SH, Cruz J, Taylor J, Bryden I, editors. Performance optimisation of a modified duck through optimal mass distribution. Proceedings of the 7th European Wave and Tidal Energy Conference; 2007.

51. Evans D. A theory for wave-power absorption by oscillating bodies. *J Fluid Mech*. 1976;77(1):1-25.

52. Lin L, Xie Y, Niu S, Wang S, Yang P-K, Wang ZL. Robust triboelectric nanogenerator based on rolling electrification and electrostatic induction at an instantaneous energy conversion efficiency of 55%. *ACS Nano*. 2015;9(1):922-930.

53. Jiang T, Tang W, Chen X, et al. Figures-of-merit for rolling-friction-based triboelectric nanogenerators. *Adv Mater Technol*. 2016;1(1):1600017.

54. Niu S, Wang ZL. Theoretical systems of triboelectric nanogenerators. *Nano Energy*. 2014;14:161.

55. Ribeiro R, Asadi E, Khamesee MB, Khajepour A. Hybrid variable damping control: design, simulation, and optimization. *Microsyst Technol*. 2014;20(8–9):1723-1732.

56. Li X, Han C, Zhang L, Wang Z. Cylindrical spiral triboelectric nanogenerator. *Nano Res*. 2015;8:3197.

57. Tang W, Zhou T, Zhang C, Fan FR, Han CB, Wang ZL. A power-transformed-and-managed triboelectric nanogenerator and its applications in a self-powered wireless sensing node. *Nanotechnology*. 2014;25(22):225402.

58. Fan F-R, Tang W, Yao Y, Luo J, Zhang C, Wang ZL. Complementary power output characteristics of electromagnetic generators and triboelectric generators. *Nanotechnology*. 2014;25(13):135402.

How to cite this article: Saadatnia Z, Asadi E, Askari H, Zu J, Esmailzadeh E. Modeling and performance analysis of duck-shaped triboelectric and electromagnetic generators for water wave energy harvesting. *Int J Energy Res*. 2017;1–13. https://doi.org/10.1002/er.3811